Acta Cryst. (1993). D**49**, 513–521

Structure of Recombinant Bovine Interferon-γ at 3.0 Å Resolution

BY CLEOPAS T. SAMUDZI* AND J. RONALD RUBIN

National Cancer Institute–Frederick Cancer Research Development Center, ABL-Basic Research Program, PO Box B, Frederick, Maryland 21702, *USA*

(*Received* 2 *December* 1992; *accepted* 2 *July* 1993)

Abstract

The three-dimensional crystal structure of recombinant bovine interferon-γ was determined using the multiple isomorphous replacement method at 3.0 Å and refined to an R factor of 19.2%. This protein crystallizes in space group $P2_12_12_1$ with unit-cell parameters of $a = 42.8$, $b = 79.9$ and $c = 85.4$ Å. There is one functional dimer in the asymmetric unit. The two polypeptide chains are related by a non-crystallographic twofold symmetry axis. The secondary structure is predominantly α-helical with extensive interdigitation of the α-helical segments of the polypeptide chains that make up the dimer. The secondary structure, tertiary structure and topology of this molecule are identical to the previously reported structures of recombinant rabbit interferon-γ and recombinant human interferon-γ. The molecular topology is also similar to that of murine interferon-β. These structural similarities strongly indicate the presence of a unique topological feature (fold) among γ-interferons from different species, and also among the different classes of interferons.

1. Introduction

Interferons are part of a complex network of regulatory cytokines that are involved in a multitude of cellular activities ranging from control of cellular function and replication, to host defense in response to infection (DeMaeyer & DeMaeyer-Guignard, 1988). There are two major classes of interferons: the type I interferons consist of the leukocyte-derived or interferon-α (IFN-α) and the fibroblast-derived or interferon-β (IFN-β), the type II interferons, also known as immune or interferon-γ (IFN-γ). This classification of interferons is based on cellular origin, biochemical properties and antigenicity (Zoon, 1987). Interferons interact with their target cells through specific cell-surface receptors. The type I interferons appear to share common receptors which are distinctly different from the type II receptors (Langer & Pestka, 1988).

Type II interferons (IFN-γ) are quite intriguing because they not only exhibit antiviral and antiproliferative activities, both in cell culture and *in vivo*, but they also show significant immunomodulatory activity. With respect to this immunoregulatory activity, IFN-γ is capable of inducing both class I and II (HLA-DR) antigens of the major histocompatibility complex and can regulate the production and expression of other cytokines and induce the differentiation of macrophages (Shalaby *et al.*, 1984; Czarniecki, Fennie, Powers & Estell, 1984; Palladino *et al.*, 1983; Svredersky, Nedwin, Goeddel & Palladino, 1985).

Much of what is presently known about the physico-chemical properties of IFN-γ is derived from experiments with the recombinant human and mouse forms (DeMaeyer & DeMaeyer-Guignard, 1988; Langer & Pestka, 1988). The coding sequence for the human IGN-γ gene encodes a 143-residue polypeptide. Following protein purification, C-terminal truncation at positions ranging from residue 127 to residue 134 has been observed (Gray *et al.*, 1982). Naturally occurring human IFN-γ is glycosylated at one or two sites. The recombinant counterpart is not glycosylated. Both C-terminal truncation and glycosylation do not appear to affect either biological activity or quartenary structure (Burton, Gray, Goeddel & Rinderknecht, 1985; Ealick *et al.*, 1991; Arakawa, Hsu, Parker & Lai, 1986). Comparison of the primary structure of human IFN-γ protein with those from other species shows sequence indentity ranging from 80 (with ovine) to 39% (with rat). The human IFN-γ is functional as a dimer in solution, and requires treatment with denaturants, such as guanidine hydrochloride or sodium dodecyl sulfate, or lowering of pH to values below 2.0 in order for dimer dissociation to occur (Le, Barrowclough & Vilcek, 1984). The stoichiometry of interaction between the human IFN-γ molecule and its receptor has been established to be one dimer of IFN-γ binding to one monomer of the extracellular domain of the receptor (Fountoulakis, Juranville, Maris, Ozmen & Garotta, 1990). Circular dichroism experiments and secondary-structure prediction techniques have suggested that the IFN-γ molecule has a

* To whom all correspondence should be directed.

ISSN 0907-4449

high (about 70%) α-helix content with approximately five or six α-helical segments per monomer, and with little or no β-structure (Chou & Fasman, 1974; Finer-Moore, Bazan, Rubin & Stroud, 1989; Denesyuk & Zav'yalov, 1982).

The crystal structure of a recombinant human IFN-γ has been reported (Ealick *et al.*, 1991). We have also previously reported a preliminary 2.7 Å resolution crystal structure of a recombinant form of rabbit interferon-γ (Samudzi, Burton & Rubin, 1991). Comparison of the crystal structures of IFN-γ molecules from these two species indicate that they are topologically identical. In both structures the predominantly α-helical dimer is made up of α-helical segments that interdigitate extensively. Such results are consistent with biochemical data and secondary-structure prediction studies. Furthermore, it is of striking interest that the crystal structures of both recombinant human and rabbit IFN-γ are truncated at their C terminus by 11 and 17 residues, respectively. This truncation is also observed in the recombinant bovine IFN-γ structure. It is probably as a result of post-translational proteolytic digestion of the molecule at the C terminus. In this report we describe the determination of the crystal structure of a recombinant bovine interferon-γ at 3.0 Å resolution.

2. Experimental procedures

Crystallization and data collection

We have previously reported the crystallization of recombinant bovine IFN-γ (Rubin & Burton, 1989). The low-resolution data to 3.7 Å for the native and heavy-atom derivatized IFN-γ crystals were collected by the ω-scan technique on a CAD-4 diffractometer using a 0.6° scan on ω with a scan speed of 0.1° min^{-1}. X-rays were produced by a high-brilliance fixed anode operating at 40 kV and 32 mA and monochromated using a graphite monochromator. Data were collected to a θ limit of 12° which corresponds to 3.7 Å resolution. 10 s local background measurements were made on both sides of individual peaks and used to determine a unique background correction for each reflection. An empirical correction for anisotropic X-ray absorption was determined from a ψ curve by measuring the intensity of the 0,10,0 reflection at $\chi = 90$ at 5° intervals on ψ and applied to the data. Three standard reflections (400, 006 and 0,10,0) were measured at 2 h intervals to monitor crystal decay during data collection.

For data collection the crystal was mounted with the long 010 axis parallel to the capillary. Area-detector data were collected using a Nicolet (Siemens) multiwire area detector. 0.25° scans on ω were carried out for each frame at a scan speed of 720 s per frame. A crystal-to-detector distance of 150 mm was used and the detector was positioned at a θ angle of 14°. Monochromatic X-rays were generated by a Rigaku RU-200 rotating-anode generator operating at 40 kV and 40 mA and a graphite monochromator. A total of 800 frames were collected. A total of 19 800 measurements of 7891 unique reflections to a resolution limit of 2.66 Å were recorded. The data were processed using the *XENGEN* programs (Howard *et al.*, 1987). The scaling between native and heavy-atom derivative data sets was done using the program *PROTEIN* (Steigeman, 1982).

Phase determination

Heavy-atom derivatives were prepared by soaking pregrown crystals in stabilizing solution containing heavy-atom compounds. The first suitable heavy-atom derivatives were obtained by soaking crystals in 1.0 m*M* K_2HgI_4 for either 1 or 4 d. A second, double derivative, was obtained by first soaking crystals in 1.0 m*M* *cis*-diaminedichloroplatinate [$K_2Pt(NH_3)_2Cl_2$] solution for 4 d followed by 1 d of soaking in 1.0 m*M* K_2HgI_4 + *cis*-$K_2Pt(NH_3)_2Cl_2$ solution.

The positions of the two major heavy-atom sites for the K_2HgI_4 derivative were determined by inspection of the $(\Delta F)^2$ Patterson maps and, subsequently, difference Fourier maps were used to locate the major platinum and mercury sites in the K_2HgI_4 + *cis*-$K_2Pt(NH_3)_2Cl_2$ double derivative. Low-resolution electron-density maps were initially computed from centroid phases using native structure-factor amplitudes weighted by their figure of merit. The 1319 terms included at 3.7 Å resolution had a figure of merit of 0.59.

Model building and refinement

A 3.7 Å resolution MIR map was calculated using phases derived from all the heavy-atom derivatives. The low-resolution map revealed all the α-helices (as rods of density) of the dimer and most of the loops connecting these α-helical segments. The two polypeptide chains are related by a non-crystallographic diad axis which also relates the positions of the major mercury and platinum sites. These 3.7 Å resolution phases were subsequently improved using the iterative isomorphous replacement (ISIR) and automated solvent-flattening procedure (Wang, 1984). The result was that the phase angles of 1622 independent terms with $I/\sigma(I) > 10.0$ (at 3.7 Å resolution) were refined to a mean figure of merit of 0.80 and used to compute electron-density maps. A polyalanine model corresponding to residues 1–119 for the first chain and 201–319 for the second chain was built into these maps using the program *FRODO* (Jones, 1978) and an Evans and Sutherland PS390

Table 1. *Summary of progress of refinement*

Stage of refinement		Resolution range (Å)	No. of reflections (2σ on I)	No. of atoms (Non-H atoms)	R factor* (%)
Initial MIR model (polyalanine)		12.0–3.7	1622†	1182 atoms, 230 residues (115 residues/monomer)	47.0
Step 1	*X-PLOR*. Rigid-body refinement of entire dimer as rigid body, followed by the two monomers, and then individual α-helices	10.0–3.7	2156	1182 atoms, 230 residues (115 residues/monomer)	41.2
Step 2	*X-PLOR*. Positional refinement	10.0–3.5	2521	1182 atoms, 230 residues (115 residues/monomer)	37.1
Step 3	*FRODO*. Model building on graphics		—	Addition of side chains	-
Step 4	*PROLSQ*. Least-squares refinement with φ and ψ in α-helices restrained	10.0–3.0	2912	1980 atoms, 238 residues (119 residues monomer)	28.4
Step 5	*FRODO*. Adjustment of model on graphics	—			
Step 6	*X-PLOR*. Simulated annealing using fast-heating (4000 K) slow-cooling protocol	10.0–3.0	2912	1980 atoms, 238 residues (119 residues/monomer)	23.6
Step 7	*FRODO*. Readjustments of model on graphics	—			—
Step 8	*PROLSQ*. Least-squares refinement with φ an ψ in α-helices restrained	8.0–3.0	2744	1980 atoms, 238 residues (119 residues/monomer)	19.2

* R factor is defined as $\sum\|F_{obs} - F_{calc}\|/\sum F_{obs}$, where F_{obs} are the observed structure-factor amplitudes from the native data and F_{calc} are the structure-factor amplitudes calculated from the model.

† To obtain the initial phases, only reflections that are 10σ on I where used.

‡ Torsion angles φ and ψ were restrained during refinement with *PROLSQ* but not with *X-PLOR*.

Table 2. *Summary of data-collection statistics for bovine IFN-γ*

	Data set	Unit-cell edges (Å) a	b	c	Resolution (Å)	% Completeness for $I > 2\sigma$	R_{sym}* (%)	R_{iso}† (%)
Diffractometer data	Native - 1	42.80	79.81	85.21	3.70	40.0	5.5	
	K_2HgI_4 + *cis*-$K_2Pt(NH_3)_2Cl_2$ (double derivative)	42.75	80.14	84.55	3.70	52.0	5.5	21.5
	K_2HgI_4 - 1	42.90	79.71	85.28	3.71	49.0	6.6	17.0
Area-detector data	Native - 2	42.80	79.90	85.40	2.90	65.0	9.3	
	K2HgI_4 - 2	42.81	80.19	86.46	2.86	74.0	7.5	24.0

* R_{sym} is given by $\sum\|I_i - \langle I\rangle\|/\sum I_i$, where I_i is the intensity of an individual measurement and $\langle I\rangle$ is the mean value for all measurements of the reflection.

† The derivative R_{iso} is given by $\sum\|I_{nat} - I_{der}\|/\sum I_{nat}$, where I_{nat} and I_{der} are the intensity measurements of the native and derivative data sets, respectively. R_{iso} reflects the mean fractional isomorphous difference in intensity between the native and derivative data sets. The double derivative [K_2HgI_4 + *cis*-$K_2Pt(NH_3)_2Cl_2$] was obtained by first soaking a recombinant bovine IFN-γ crystal for 4 d in saturated *cis*-$K_2Pt(NH_3)_2Cl_2$, followed by a 20 h soak of the same crystal in 10% saturated K_2HgI_4 solution. Only one crystal was used per data set.

molecular graphics display system. Comparison of the calculated structure factors based on this polyalanine model with the observed structure amplitudes yielded an R factor of 0.47 for the 3.7 Å resolution data. Starting with the 3.7 Å resolution native phases, phase extension was performed to 3.0 Å using the ISIR procedure. Difference electron-density maps ($F_o - F_c$) using the polyalanine model and 3.0 Å resolution data revealed more details of the course of the polypeptide chains in the loop regions of the molecule as well as density corresponding to amino-acid side chains extending out from C^β atoms of the polyalanine model. Most of the amino-acid side chains were then fitted to the polyalanine model based on these maps.

The refinement of the model was carried out in steps, each involving a number of cycles using a least-squares refinement program, *PROLSQ* (Hendrickson & Konnert, 1980) and a general purpose molecular dynamics refinement package, *X-PLOR* (Brünger, Kuriyan & Karplus, 1987). This was followed by manually adjusting the model using the *FRODO* program on the molecular graphics system. At the end of each refinement step, difference Fourier maps with coefficients $2|F_o| - |F_c|$ and $|F_o| - F_c$ and with calculated phases (α_c) were computed to check the course of refinement and to rebuild portions of the molecule as needed. Table 1 summarizes the refinement. Individual temperature factors were introduced and refined in step 8, thus accounting for the 4.4% change in R factor from the previous step. As model building and refinement progressed, the new model was compared with the original 3.7 Å MIR map.

3. Results and discussion

General

Diffractometer data were used initially in the structure determination to survey and refine the parameters of potential heavy-atom derivatives. Bijvoet pairs were merged for all data. Table 2 summarizes the data-collection satistics for both native data and heavy-atom derivative data sets. Table 3 shows the Cullis R factor at 3.7 Å resolution for both heavy-atom derivatives after several cycles of heavy-atom refinement. Fig. 1 shows a portion of the 3.7 Å

Table 3. *Summary of heavy-atom derivative search and their final positions*

Derivative	Site number	Relative occupancy*	x	y	z	Cullis R factor† (%)
K_2HgI_4	Hg - 1	184.3	0.000	0.193	0.856	
	Hg - 2	133.9	0.387	0.471	0.572	50.6
	Hg - 1	176.9	0.000	0.193	0.850	
K_2HgI_4 +	Hg - 2	190.1	0.390	0.472	0.572	51.2
cis-$Pt(NH_3)_2Cl_2$	Pt - 1	112.3	0.161	0.561	0.959	
(double derivative)	Pt - 2	130.5	0.844	0.269	0.846	

* The relative occupancy is in arbitrary units and heavy-atom sites are in fractional coordinates. The native and derivative data sets were pre-scaled together with a single scale in this case.

† The Cullis R factor is a measure of the goodness of phases derived from a particular heavy-atom derivative, it is given by $\Sigma_l(F_{PH} \pm F_P) - F_H|/\Sigma|F_{PH} - F_P|$; where F_{PH} is the structure factor of the heavy-atom derivative data, F_P is the structure factor of native protein and F_H is the heavy-atom contribution.

resolution solvent-flattened multiple isomorphous replacement (MIR) electron-density map. This map (contoured at 1σ) is calculated from the MIR data shown in Table 3. The map shows a portion of the longest α-helix (helix C), loop III and helix D of one monomer. The continuity and clarity of this portion of the map is representative of the entire map. Rods of high electron density corresponding to α-helical segments are clearly visible. These electron-density maps revealed most of the course of the two polypeptide chains (about 115 residues per chain). Fig. 2. shows a corresponding region of the final 3.0 Å $2F_o - F_c$ electron-density map (contoured at 1σ) calculated, as described in the previous section, after several cycles of refinement and fitting of side chains.

Native area-detector data were used for refinement of the model. Table 1 shows a summary of the progress of refinement. Individual B factors were included only in step 8. Fig. 3 shows the Ramachandran plot (Ramakrishnan & Ramachandran, 1965) of the φ–ψ conformational torsion angles of the final model. Most of the φ–ψ angles are in or very near the allowed regions. Only seven out of 238 residues have φ–ψ angles that deviate significantly from allowed regions. These residues (indicated by $\triangle$) are Ser18, Ser19, Lys53, Lys61, Ile98 and Gln297. They are located either in loops or at the N-terminal of C-terminal end of α-helices. Table 4 gives the rest of the final geometry of the model. The coordinates for all atoms of this model have been

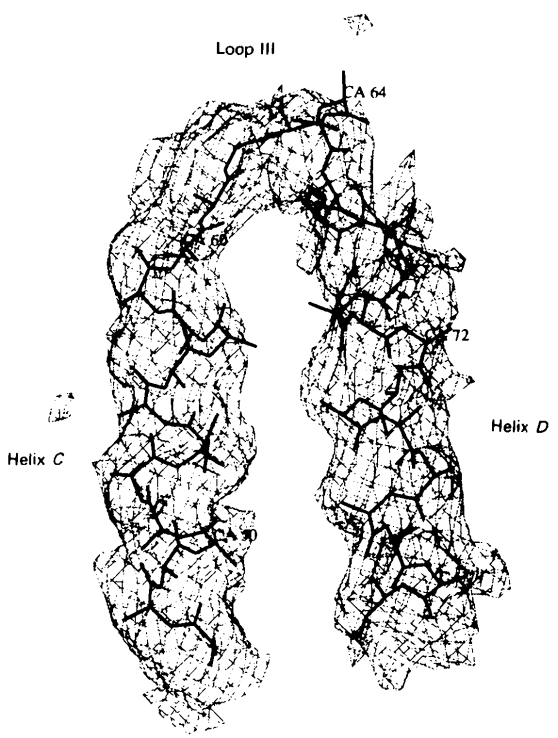

Fig. 1. A 3.7 Å resolution solvent-flattened multiple isomorphous replacement (MIR) electron-density map of recombinant bovine IFN-γ contoured at 1.0σ level. The polyalanine model of helix C–loop II–helix D is fitted into a continuous segment of electron density.

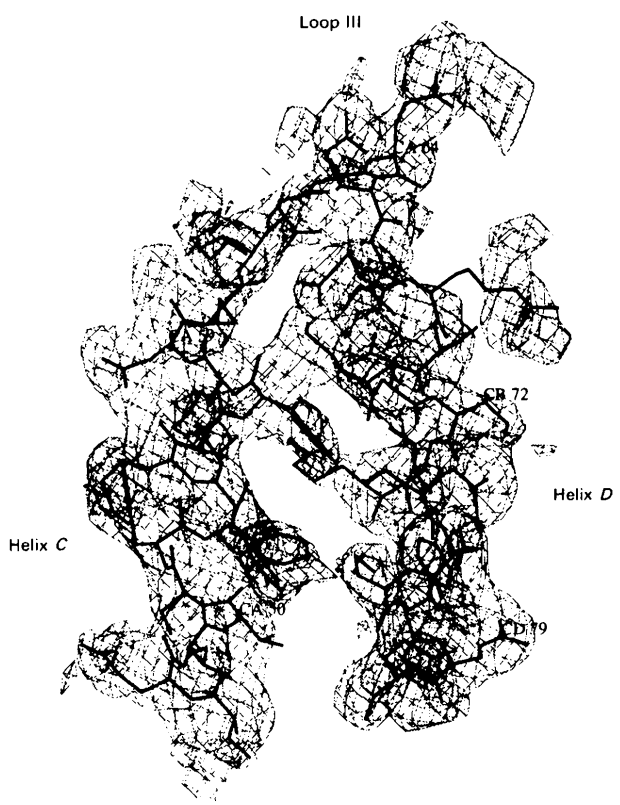

Fig. 2. The final 3.0 Å resolution ($2|F_o - F_c|$) electron-density map for recombinant bovine IFN-γ showing the same segment of structure (helix C–loop III–helix D) as in Fig. 1, and also contoured at 1.0σ level. The continuity and clarity of this region of the map is representative of the entire map.

deposited in the Protein Data Bank (Bernstein *et al.*, 1977).*

Secondary structure organization

The organization of the secondary structure of the recombinant bovine IFN-γ dimer is identical to that of the recombinant human and rabbit IFN-γ (Ealick *et al.*, 1991; Samudzi *et al.*, 1991). The dimer is shaped like a prolate ellipsoid with approximate dimensions 60 × 40 × 30 Å. It is comprised of two identical polypeptide chains related by a non-crystallographic twofold axis. One polypeptide chain with residues numbered from 1–119 is made up of six α-helices (designated *A* through *F*) connected by loops of varying lengths (designated I–V). The second chain has residues numbered 201–319. Its α-helices are designated *A'* through *F'*, and its corresponding loops are also designated I'–V'. The dimer structure is organized into two structural domains. Each domain consists of a six α-helical bundle. Four of the α-helical segments within the domain are contributed by one chain of the dimer, while the remaining two α-helical segments are contributed by the other chain (See Fig. 4). This arrangement gives rise to both parallel and anti-parallel α-helical segments with close packing of adjacent α-helices. In addition, four of the α-helices (two from each monomer) in the domain form an interdigitating helix–loop–helix core. Thus, the segment helix *B*–loop II–helix *C* from one monomer interlocks with the segment helix *E'*–loop V'–helix *F'* from the other monomer as illustrated in stereo in Fig. 5.

* Atomic coordinates have been deposited with the Protein Data Bank, Brookhaven National Laboratory (Reference: 1RFB). Free copies may be obtained through The Technical Editor, International Union of Crystallography, 5 Abbey Square, Chester CH1 2HU, England (Supplementary Publication No. SUP 37093). A list of deposited data is given at the end of this issue.

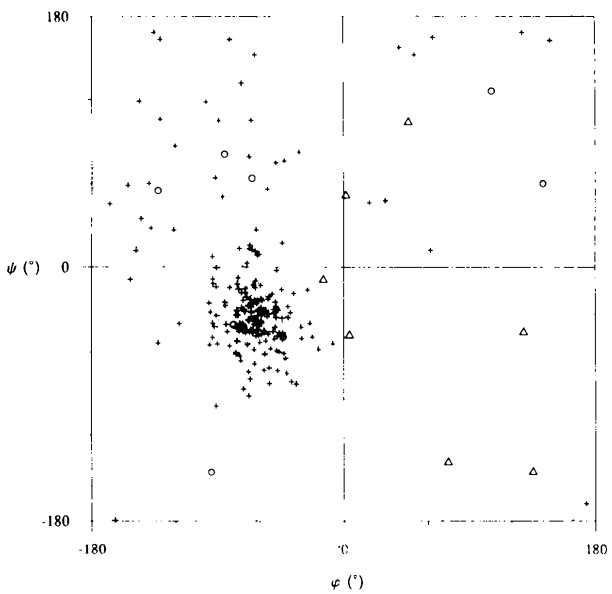

Fig. 3. Ramachandran plot for recombinant bovine IFN-γ dimer: (○) glycyl residues, (+) residues falling in or near allowed regions, (△) residues in disallowed regions.

Table 4. *Summary of final statistics of refinement*

R factor (%)	19.2
Weights*	$w = \sigma_F^{-2}$
Resolution (Å)	8.0–3.0
No. of reflections	2744
No. of atoms	1980
No. of residues	119
No. of water molecules	0
Distance restraints† (Å)	
Bond distance	0.017 (0.020)
Angle distance	0.052 (0.030)
Planar 1 4 distance	0.102 (0.050)
Plane restraints (Å)	0.016 (0.020)
Chiral-center restraints (Å^3)	0.162 (0.060)
Non-bonded restraints	
Single torsion contact (Å)	0.254 (0.300)
Multiple torsion contact (Å)	0.355 (0.300)
Possible (*X*...*Y*) hydrogen bond (Å)	0.322 (0.300)
Conformational torsion angles ( )	
Planar	11.8 (2.5)
Staggered	24.8 (6.0)
Orthonormal	50.6 (20.0)
B_{iso} restraints‡ (Å^2)	
Main-chain bond	3.484 (2.300)
Main-chain angle	6.071 (2.500)
Side-chain bond	3.780 (3.500)
Side-chain angle	5.937 (4.000)
Hydrogen bond	17.988 (10.000)

* $\sigma_F = (25.0) + (-50)(s - 1/6)$, $s = \sin(\theta)/\lambda$.
† Root-mean-square deviations from ideality are followed by their respective target restraints in parentheses.
‡ Isotropic temperature (thermal) factors.

Structure–function implications

Although the two polypeptide chains are related by a non-crystallographic twofold symmetry, the lengths of corresponding α-helical segments in each chain are identical. The twofold restraints were not used in refinement. The root-mean-square difference for the C^α atoms between the two non-crystallographically related monomers is 0.06656; and that for the main-chain atoms is 0.06962. The greatest differences lie in the loops. Therefore, any description referring to one monomer also applies to the other. At 3.0 Å resolution, the local differences are very small and confined to longer side chains. The six α-helices vary in length from the longest helix (helix *C*) consisting of 16 residues to the shortest helix (helix *B*) with only seven residues. Fig. 6 shows a comparison of the primary structures of IFN-γ from nine sources. The secondary-structure elements for the three molecules whose three-dimensional structures are now known (rabbit, bovine and human) are also shown. The six α-helices in the recombinant bovine IFN-γ are made up of the following residues: helix *A* (7–16); helix *B* (27–34); helix *C* (45–58); helix *D* (65–82); helix *E* (87–96); and helix *F* (108–116).

Helix *F* shows the greatest difference between the rabbit and bovine structures on the one hand, and the human structure on the other hand. In both rabbit and bovine cases, residues 104–107 and 117–119 do not exhibit α-helical (not even 3_{10}-helical or π-helical) character. Even when strictly constrained as part of α-helices during refinement, these regions continue to remain non-helical.

One criterion for evaluating a three-dimensional structure is the extent to which hydrophobic residues are exposed on the surface of the molecule and hydrophobic residues are buried. In the recombinant bovine IFN-γ dimer, most of the helices are accessible to the surface of the molecule and are also amphipathic. The exception, helix *C*, is buried in the interior of the dimer and contains a highly conserved hydrophobic stretch of residues (with the exception of a serine residue): Ile49-Val50-Ser51-Phe52-Tyr53-Phe54. Potential *N*-glycosylation sites are located at residues Asn16 and Asn83. The former is at the C-terminal end of helix *A* and the latter at the amino terminus of helix *E*. Both are exposed on the surface of the molecule.

The correlation between structure and biological activity of this molecule has primarily employed such techniques as monoclonal and polyclonal antibodies, partial proteolytic digestion and recombinant-DNA techniques. Several studies have suggested the involvement of the C terminus and N terminus in antiviral and antiproliferative activity (Caruso *et al.*, 1992; Alfa & Jay, 1988; Ziai *et al.*, 1986). Biological activity can be separated into four distinct components namely receptor binding, antiviral activity, antiproliferative activity, and immunomodulatory function. Two separate groups, Alfa and coworkers and Ziai and coworkers (Alfa & Jay, 1988; Ziai *et al.*, 1986) have proposed from their findings that the recombinant human IFN-γ contains two distinct functional domains: (1) a receptor-binding domain

Fig. 4. Priestle ribbons cartoon model of the recombinant bovine IFN-γ dimer with two views showing the organization of α-helices. The two views are at right angles to each other. The top view is parallel to the dimer dyad, and the bottom view is perpendicular to the dimer dyad.

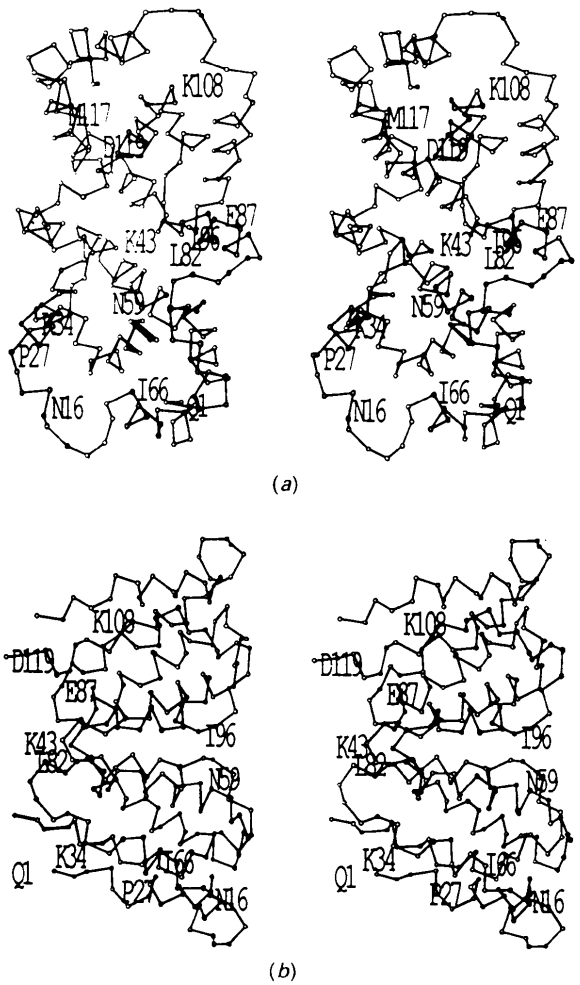

Fig. 5. Stereo diagrams showing the C$^{\alpha}$ tracing of the recombinant bovine IFN-γ. Only one polypeptide chain is labelled at the following points: the N-terminal residue, the C-terminal residue, and the beginning and end of α-helices. (*a*) View down the dimer dyad, (*b*) view perpendicular to the dimer dyad.

and (2) a domain responsible for antiviral activity, cell-growth inhibition and enhancement of HLA-antigen expression. Furthermore, there is evidence that the binding of the IFN-γ molecule to its receptor on the cell surface is not sufficient to produce a physiological response. There is evidence for the requirement of species-specific (possibly transmembrane) accessory-factor protein with an extracellular domain that interacts with the IFN-γ dimer and/or the extracellular domain of IFN-γ receptor (Hibino, Mariano, Kumar, Kozak & Pestka, 1991). Therefore, for full biological activity of IFN-γ, the following three components are necessary: (1) the IFN-γ dimer, (2) the IFN-γ receptor and (3) the accessory factor. A combination of biochemical data and the three-dimensional structure presented in this report lead us to postulate a model for the interaction of IFN-γ with response elements on the cell surface. Since the IFN-γ structure consists of distinct and identical domains separated by a deep cleft (see Figs. 4 and 5), we propose a possible model that utilizes the twofold symmetry of the dimer and thus allows both termini to interact with the receptor and the accessory factor (Fig. 7).

Comparison with other interferons

Fig. 6 is a comparison of the IFN-γ sequences from a variety of species. In Fig. 6, completely conserved residues are shown in white letters with black background, while conservative substitutions are shown in gray. The average sequence identity between bovine IFN-γ and IFN-γ from five other species (human, porcine, ovine, canine and rabbit) is 75% (see Table 5). However, sequence identity between bovine IFN-γ and the remaining two species (mouse and rat) is significantly lower (44%). The structure of recombinant rabbit IFN-γ is topologically identical to the structure described in this report. A similar packing of α-helices was also observed in the structure of recombinant mouse IFN-β (Senda *et al.*, 1990). The major difference between IFN-β and the IFN-γ is that the IFN-β is a monomer and does not have the interdigitating helix–loop–helix core, with the two segments from different polypeptide chains, and IFN-β has only five α-helices. The topological identity of the three known IFN-γ crystal structures (human, rabbit and bovine), together with high sequence similarity with

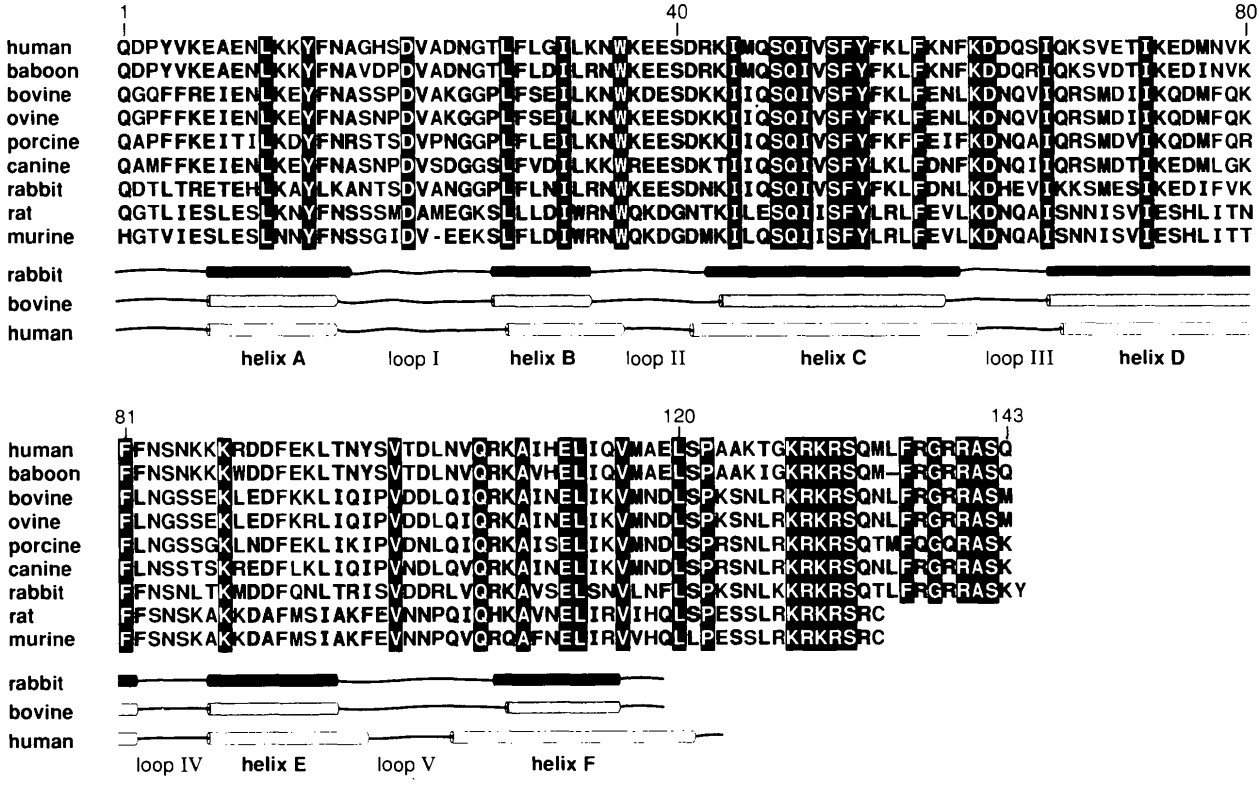

Fig. 6. Comparison of IFN-γ sequences from a number of species. Sequence alignment showing regions with completely conserved residues in white letters with black background, and those with conservative substitutions in gray. Secondary-structure elements for rabbit, bovine and human IFN-γ are also shown .

the other IFN-γ molecules (Table 5 and Fig. 6) are sufficient reason to expect the same characteristic helical fold among all of the other γ-interferons.

Crystal packing

The recombinant bovine interferon-γ dimers are tightly packed in the crystal lattice. Fig. 8 shows that each dimer utilizes practically all the six 'faces' of the prolate ellipsoid in forming contacts with neighboring dimer molecules. This tight packing is consistent with the previously reported low solvent content (42%) computed for these crystals (Rubin & Burton, 1989), and does not allow for additional space to accommodate a disordered C terminus and thus indicating that indeed a large portion of the C terminus was cleaved off. Furthermore, this mode of packing contrasts with the one found in the hexagonal crystals of recombinant rabbit IFN-γ where large solvent channels of about 40 Å in diameter were found running parallel the longest axis (*c* axis), and the dimer utilized only five or six possible surfaces for dimer–dimer interactions (Samudzi *et al.*, 1991).

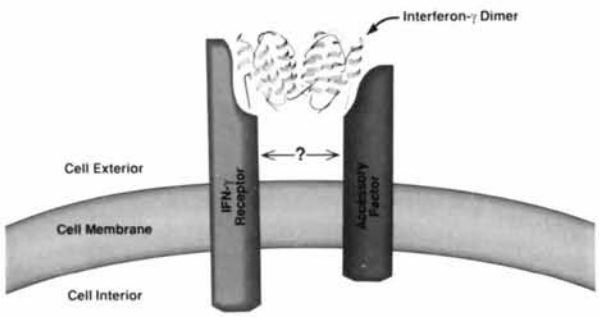

Fig. 7. Model for IFN-γ–IFN-γ-receptor–accessory factor complex. The model maximizes the twofold symmetry of the IFN-γ dimer. Note, however, that the IFN-γ receptor and the accessory factor do not necessarily use similar contacts to interact with the IFN-γ dimer. Furthermore, it is not clear whether or not the IFN-γ receptor and the accessory factor make direct contact with each other intracellularly or extracellularly.

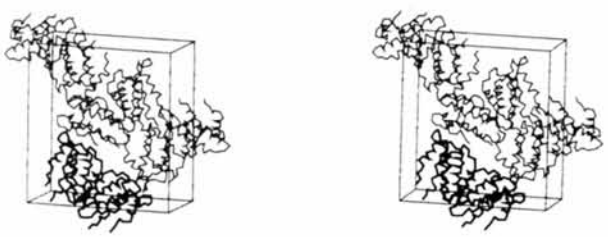

Fig. 8. The stereo diagram showing packing of recombinant bovine IFN-γ dimers in the crystallographic unit cell. The tight packing does not accommodate additional space for a disordered C terminus.

Table 5. *Degree of protein-sequence identity* (%) *among* IFN-γ *molecules*

	Human	Baboon	Bovine	Ovine	Porcine	Canine	Rabbit	Rat	Murine
Human	—								
Baboon	92	—							
Bovine	60	59	—						
Ovine	77 (80)*	60	96 (96)	—					
Porcine	59 (75)	57	78	79	—				
Canine	65 (76)	63	76	81	72	—			
Rabbit	67	64	64	64	58	59	—		
Rat	39 (60)	39	45	44	44	42 (65)	38	—	
Murine	39	39	43	43	43	40 (63)	38	87 (90)	—

* Coding region nucleotide-sequence homology in parentheses.

The authors would like to thank Drs A. A. Kossiakoff, L. Sjölin and R. M. Stroud for many helpful discussions. This research was sponsored by the National Cancer Institute, DHHS, under contract No. N01-CO-74101 with ABL-Basic Research Program. The contents of this publication do not necessarily reflect the views or policies of the Department of Health and Human Services, nor does mention of trade names, commercial products, or organizations imply endorsement by the US Government.

References

ALFA, M. J. & JAY, F. T. (1988). *J. Immunol.* **141**, 2474–2479.

ARAKAWA, T., HSU, Y.-R., PARKER, C. G. & LAI, P.-H. (1986). *J. Biol. Chem.* **261**, 8534–8537.

BERNSTEIN, F. C., KOETZLE, T. F., WILLIAMS, G. J. B., MEYER, E. F. JR, BRICE, M. D., RODGERS, J. R., KENNARD, O., SHIMANOUCHI, T. & TASUMI, M. (1977). *J. Mol. Biol.* **112**, 535–542.

BRÜNGER, A., KURIYAN, J. & KARPLUS, M. (1987). *Science*, **235**, 458–460.

BURTON, L. E., GRAY, P. W., GOEDDEL, D. V. & RINDERKNECHT, E. (1985). *Biology of the Interferon System*, edited by H. KIRCHNER & H. SCHELLEKENS, pp. 403–409. Amsterdam: Elsevier.

CARUSO, A., VIANI, E., TIBERIO, L., POLLARA, P., MONTI, E., BONFANTI, C., GAO, J., LANDOLFO, S., BALSARI, A. & TURANO, A. (1992). *J. Interferon Res.* **12**, 49–54.

CHOU, P. Y. & FASMAN, G. D. (1974). *Biochemistry*, **13**, 211–222.

CZARNIECKI, C. W., FENNIE, C. W., POWERS, D. B. & ESTELL, D. A. (1984). *J. Virol.* **49**, 490–496.

DEMAEYER, E. & DEMAEYER-GUIGNARD, J. (1988). *Interferons and Other Regulatory Cytokines*, pp. 1–4, 336–350. New York: John Wiley.

DENESYUK, A. I. & ZAV'YALOV, V. P. (1982). *Immunol. Lett.* **5**, 223–226.

EALICK, S. E., COOK, W. J., VIJAY-KUMAR, S., CARSON, M., NAGABHUSHAN, T. L., TROTTA, P. P. & BUGG, C. E. (1991). *Science*, **252**, 698–702.

FINER-MOORE, J., BAZAN, J. F., RUBIN, J. R. & STROUD, R. M. (1989). *Prediction of Protein Structure and the Principles of Protein Conformation*, edited by G. D. FASMAN, pp. 719–759. New York: Plenum Press.

FOUNTOULAKIS, M., JURANVILLE, J.-F., MARIS, A., OZMEN, L. & GAROTTA, G. (1990). *J. Biol. Chem.* **265**, 19758–19767.

GRAY, P. W., LEUNG, D. W., PENNICA, D., YELVERTON, E., NAJARIAN, R., SIMONSON, C., DERYNCK, R., SHERWOOD, P. J., WALLACE, D. M, BERGER, S. L., LEVINSON, A. D. & GOEDDEL, D. V. (1982). *Nature (London)*, **295**, 503–508.

HENDRICKSON, W. A. & KONNERT, J. H. (1980). *Biomolecular Structure, Function, Conformation and Evolution*, edited by R. SRINIVASAN, pp. 43–57. Oxford: Pergamon Press.

HIBINO, Y., MARIANO, T. M., KUMAR, C. S., KOZAK, C. A. & PESTKA, S. (1991). *J. Biol. Chem.* **266**, 6948–6951.

HOWARD, A. J., GILLILAND, G. L., FINZEL, B. C., POULOS, T. L., OHLENDORF, D. H. & SALEMME, F. R. (1987). *J. Appl. Cryst.* **20**, 383–387.

JONES, T. A. (1978). *J. Appl. Cryst.* **11**, 268 272.

LANGER, J. A. & PESTKA, S. (1988). *Immunol. Today*, **9**, 393 400.

LE, J., BARROWCLOUGH, B. S. & VILCEK, J. (1984). *J. Immunol. Methods*, **69**, 61–70.

PALLADINO, M. A., SREDERSKY, L. P., SHEPARD, H. M., PEARLSTEIN, K. T., VILCEK, J. & SCHEID, M. P. (1983). *Interferon Research: Clinical Application and Regulatory Consideration*, edited by K. C. ZOON, pp. 139–147. Amsterdam: Elsevier.

RAMAKRISHNAN, C. & RAMACHANDRAN, G. N. (1965). *Biophys. J.* **5**, 909–933.

RUBIN, J. R. & BURTON, L. E. (1989). *J. Mol. Biol.* **209**, 829–831.

SAMUDZI, C. T., BURTON, L. E. & RUBIN, J. R. (1991). *J. Biol. Chem.* **266**, 21791–21797.

SENDA, T., MATSUDA, S., KURIHARA, H., NAKAMURA, K. T., KAWANO, G., SHIMIZU, H., MIZUNO, H. & MITSUI, Y. (1990). *Proc. Jpn. Acad. Ser. B*, **66**, 77–82.

SHALABY, M. R., WECK, P. K., RINDERKNECHT, E., HARKINS, R. N., FRANE, J. W. & ROSS, M. J. (1984). *Cell Immunol.* **81**, 380–392.

STEIGEMAN, W. (1982). In *PROTEIN. A Package of Crystallographic Programs for the Analysis of Proteins*, edited by R. HUBER. MPI für Biochemie, D8033 Martinsried, Germany.

SVREDERSKY, L. D., NEDWIN, G. E., GOEDDEL, D. V. & PALLADINO, M. A. (1985). *J. Immunol.* **134**, 1604–1608.

WANG, B.-C. (1984). *Methods Enzymol.* **115**, 90–112.

ZIAI, M. R., IMBERTI, L., KOBAYASHI, M., PERUSSIA, B., TRINCHIERIE, G. & FERRONE, S. (1986). *Cancer Res.* **46**, 6187–6190.

ZOON, K. C. (1987). *Hum. Interferons Struct. Funct.* **9**, 1–12.